Real-Time Decentralized Control of a Hardware-In-the-Loop Microgrid

Maximiliano Bueno-Lopez, Eduardo Giraldo

Abstract—In this work, a novel real-time decentralized control approach of a Hardware-In-the-Loop (HIL) microgrid is presented. A state-space feedback control signal is designed based on an optimal Linear Quadratic Regulator control. The states of the microgrid are estimated using a Kalman-Bucy observer. In order to evaluate the performance of the proposed decentralized controller method, the microgrid and the controller are designed and evaluated in simulation and also in a real-time Hardware-In-the-Loop environment. In addition, the performance of a centralized controller based on state feedback is also implemented and evaluated over the simulated and HIL microgrid for comparative analysis.

Index Terms—Control, decentralized, microgrid, real-time.

I. INTRODUCTION

THE hierarchical structure of the microgrid control is divided into primary, secondary, and tertiary. In the primary control, the stability of the microgrid voltage and frequency must be guaranteed. In the secondary control, the main goal is to refine the primary control, compensating deviations in the frequency and voltage. Finally, the tertiary control deals with the optimal operation of the system with the power flow control in the microgrid. In the present article, the contribution is oriented towards primary control [1], [2]. The challenges in the field of control systems have made microgrids evolve, more data monitoring and visualization tools are incorporated, and its validation is needed [3]. For this purpose, real-time Digital Simulator (RTDS) and Simulink have been used, especially to analyze the performance and control of microgrids [4]. These tools demonstrate the operation of the system and can be used as validation of the proposed control strategies through a Hardware-In-the-Loop (HIL) simulation [2], [5], [6]. RTDS operates continuously in real-time, which means that analytical studies can be performed much faster than offline simulation programs.

The adaptive control strategies allow continuous update of the system parameters and the design variability in terms of the identified model [7]. The control of systems with non-linearities around an operational point also can be performed by adaptive linear control techniques [8], [9] or by intelligent neural networks based control [10]. In [11], an ARMAX based methodology for identifying and controlling multivariable time-varying systems is proposed, based on

Maximiliano Bueno-Lopez is an associate professor at the Department of Electronics, Instrumentation, and Control, Universidad del Cauca, Popayan, Colombia. E-mail: mbuenol@unicauca.edu.co

Eduardo Giraldo is a full professor at the Department of Electrical Engineering, Universidad Tecnológica de Pereira, Pereira, Colombia. Research group in Automatic Control. E-mail: egiraldos@utp.edu.co

a pole placement technique. It can be seen that the multivariable system can effectively track any set point under noise conditions. However, the model is designed only for systems with an equal number of inputs and outputs.

A useful approach to model any multivariable system, like a microgrid, by state-space equations is presented in [12]. A set of first-order differential equations is proposed to describe the system dynamics. Several attempts to model microgrids and smart grids in state-space have been presented [13], [14], [15], [16], [17]. For example, in [17] a smart grid with decentralized control is proposed in state space. However, these approaches are model dependant and require detailed knowledge of the system to be controlled. Finally, in [18] a nonlinear control designed based on a microgrid model s presented.

In this work, a decentralized controller for an inter-connected microgrid is presented based on a state-feedback approach computed by an optimal Linear Quadratic Regulator and a state estimation based on a Kalman-Bucy observer. The proposed method is evaluated in simulation under noise conditions and in real-time by using a HIL structure. The main contributions of this paper are the control strategies implemented and tested in a Real-Time Digital Simulator (RTDS) with controller hardware in the loop. The paper is organized as follows: in section II a mathematical description of the microgrid is presented in state space. In section III the centralized and decentralized control structures by including the Kalman-Bucy observer are presented. In section IV a detailed description of the HIL structure is presented, and finally, in section V the experimental results for simulated microgrid and HIL system are discussed.

II. STATE-SPACE DESCRIPTION OF A MICROGRID

In this paper, an inter-connected microgrid with three subsystems is considered, as depicted in Fig. 1. The microgrid includes three distributed energy resources (DERs) interfaced with the local load through a converter. The first DER represents a photovoltaic solar generator in series with a voltage source converter (VSC), and the other two correspond to a hybrid wind-solar system. Variables V_{d1}, V_{d2}, and V_{d3} represent the voltage injected by each DER into the microgrid.

A general dynamic modeling of the microgrid of Fig. 1 is presented in (1), according to the model in [19] as follows:

$$\dot{x} = Ax(t) + Bu(t) + \eta(t) \tag{1}$$

being x the state vector, u the input vector, and ω the disturbance vector, A the feedback matrix, B the input matrix, η the state noise, and where (1) is used to describe the dynamic behavior of the microgrid.
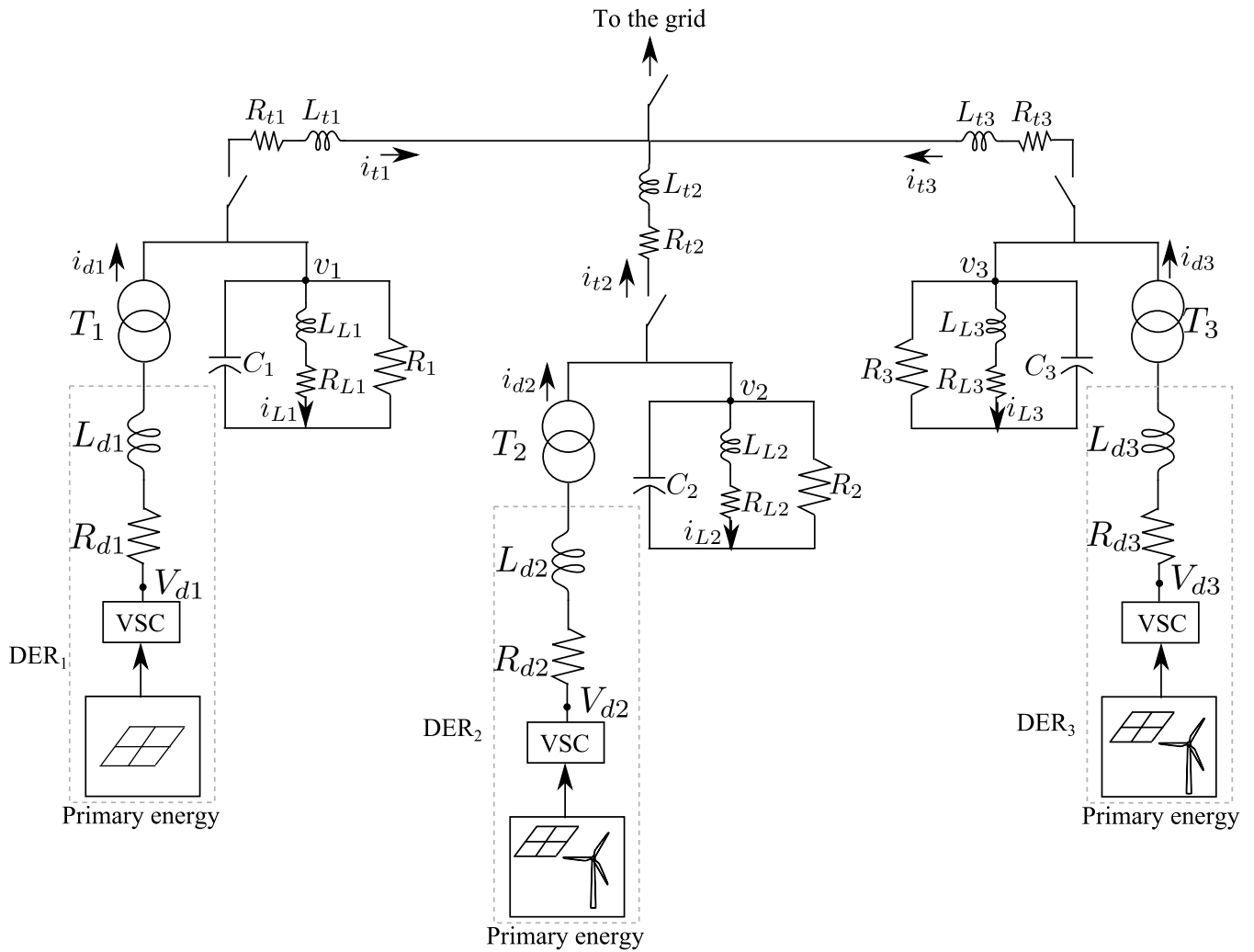
Fig. 1. Inter-connected microgrid structure

According to (1) and the microgrid of Fig. 1, with $R_{t3} = 0$ and $L_{t3} = 0$], the feedback matrix A is defined as follows:

$$A = \begin{bmatrix} A_{11} & A_{12} & A_{13} \\ A_{21} & A_{22} & A_{23} \\ A_{31} & A_{32} & A_{33} \end{bmatrix}$$

being

$$A_{11} = \begin{bmatrix} -\frac{R_{L1}}{L_{L1}} & 0 & 0 & \frac{1}{L_{L1}} \\ 0 & -\frac{R_{d1}}{L_{d1}} & 0 & -\frac{1}{L_{d1}} \\ 0 & 0 & -\frac{R_{t1}}{L_{t1}} & \frac{1}{L_{t1}} \\ -\frac{1}{C_1} & -\frac{1}{C_1} & -\frac{1}{C_1} & -\frac{1}{R_1 C_1} \end{bmatrix}$$

and

$$A_{22} = \begin{bmatrix} -\frac{R_{L2}}{L_{L2}} & 0 & 0 & \frac{1}{L_{L2}} \\ 0 & -\frac{R_{d2}}{L_{d2}} & 0 & -\frac{1}{L_{d2}} \\ 0 & 0 & -\frac{R_{t2}}{L_{t2}} & \frac{1}{L_{t2}} \\ -\frac{1}{C_2} & -\frac{1}{C_2} & -\frac{1}{C_2} & -\frac{1}{R_2 C_2} \end{bmatrix}$$

and

$$A_{33} = \begin{bmatrix} -\frac{R_{L3}}{L_{L3}} & 0 & \frac{1}{L_{L3}} \\ 0 & -\frac{R_{d3}}{L_{d3}} & -\frac{1}{L_{d3}} \\ -\frac{1}{C_3} & -\frac{1}{C_3} & -\frac{1}{R_3 C_3} \end{bmatrix}$$

with A_{11}, A_{22} and A_{33} the three microgrids feedback matrices, with inter-connections defined by the A_{ij} matrices,

as follows:

$$A_{12} = \begin{bmatrix} 0 & 0 & 0 & 0 \\ 0 & 0 & 0 & 0 \\ 0 & 0 & 0 & -\frac{1}{L_{t1}} \\ 0 & 0 & 0 & 0 \end{bmatrix}$$

and

$$A_{23} = \begin{bmatrix} 0 & 0 & 0 \\ 0 & 0 & 0 \\ 0 & 0 & -\frac{1}{L_{t2}} \\ 0 & 0 & 0 \end{bmatrix}$$

and $A_{13} = 0$, $A_{23} = 0$, $A_{31} = 0$ and $A_{32} = 0$. It is worth mentioning that a zero matrix in the feedback matrix A_{ij} implies no interconnection between the i and j microgrids.

In addition, the input matrix B is defined as

$$B = \begin{bmatrix} B_{11} & B_{12} & B_{13} \\ B_{21} & B_{22} & B_{23} \\ B_{31} & B_{32} & B_{33} \end{bmatrix}$$

with

$$B_{11} = \begin{bmatrix} 0 \\ \frac{1}{L_{d1}} \\ 0 \\ 0 \end{bmatrix}, B_{22} = \begin{bmatrix} 0 \\ \frac{1}{L_{d2}} \\ 0 \\ 0 \end{bmatrix}, B_{33} = \begin{bmatrix} 0 \\ \frac{1}{L_{d3}} \\ 0 \end{bmatrix}$$

and $B_{12} = 0$, $B_{13} = 0$, $B_{21} = 0$, $B_{23} = 0$, $B_{31} = 0$ and $B_{32} = 0$. As before, it is worth noting that a zero input matrix B_{ij} implies that the $i-$th input has no influence in the $j-$th microgrid. with control inputs for each subsystem of the microgrid defined as

$$u = \begin{bmatrix} V_{d1} \\ V_{d2} \\ V_{d3} \end{bmatrix} \quad (2)$$

and the state-space vector defined as

$$x = \begin{bmatrix} x_1 \\ x_2 \\ x_3 \end{bmatrix} \quad (3)$$

being

$$x_1 = \begin{bmatrix} i_{L1} \\ i_{d1} \\ i_{t1} \\ v_1 \end{bmatrix}, x_2 = \begin{bmatrix} i_{L2} \\ i_{d2} \\ i_{t2} \\ v_2 \end{bmatrix}, x_3 = \begin{bmatrix} i_{L3} \\ i_{d3} \\ v_3 \end{bmatrix} \quad (4)$$

Assuming that the outputs of the microgrid are the Point-Common-Coupling (PCC) v_i voltages, the measurement equation can be defined as

$$y(t) = Cx(t) \quad (5)$$

being

$$y = \begin{bmatrix} v_1 \\ v_2 \\ v_3 \end{bmatrix} \quad (6)$$

with C defined as

$$C = \begin{bmatrix} C_{11} & 0 & 0 \\ 0 & C_{22} & 0 \\ 0 & 0 & C_{33} \end{bmatrix}$$

and

$$C_{11} = C_{22} = \begin{bmatrix} 0 & 0 & 0 & 1 \end{bmatrix}$$
$$C_{33} = \begin{bmatrix} 0 & 0 & 1 \end{bmatrix}$$

The state-space model of (1) can be represented in discrete time as a linear difference equation by using a zero-order-hold method, resulting in the following discrete state-space equation

$$x[k+1] = Fx[k] + Gu[k] + \eta[k] \quad (7)$$

where $F = \exp A t_s$, $G = \int \exp A \tau d\tau B$ being t_s the sample time, $t_k = k t_s$, and being k the sample, with

$$F = \begin{bmatrix} F_{11} & F_{12} & F_{13} \\ F_{21} & F_{22} & F_{23} \\ F_{31} & F_{32} & F_{33} \end{bmatrix}$$

and

$$G = \begin{bmatrix} G_{11} & G_{12} & G_{13} \\ G_{21} & G_{22} & G_{23} \\ G_{31} & G_{32} & G_{33} \end{bmatrix}$$

III. CONTROL STRATEGY

To design the state regulator, the strategy described in this section has been followed. It is worth mentioning that the voltages V_{di} are the control signals and correspond to the $i-$th voltage of each of the DERs. The state feedback control law can be defined, for a centralized control structure in discrete time, as follows

$$u[k] = -K_d x[k] \quad (8)$$

being

$$K_d = \begin{bmatrix} K_{d11} & K_{d12} & K_{d13} \\ K_{d21} & K_{d22} & K_{d22} \\ K_{d31} & K_{d32} & K_{d33} \end{bmatrix} \quad (9)$$

By considering a Linear-Quadratic-Regulator the K_d gain can be computed as

$$F^T S F - S - F^T S G (G^T S G + R)^{-1} G^T S F + Q = 0$$
$$K_d = (G^T S G + R)^{-1} G^T S F$$

being Q and R constrain matrices.

In this work a decentralized structure is proposed where the $i-$th control signal can be computed as

$$u_i[k] = -K_{dii} \tilde{x}_i[k] \quad (10)$$

being $\tilde{x}_i[k]$ the estimated state space variable of the $i-$th microgrid at sample k. Also, by considering a Linear-Quadratic-Regulator the K_{dii} gain can be computed as

$$F_{ii}^T S F_{ii} - S - F_{ii}^T S G_{ii} (G_{ii}^T S G_{ii} + R)^{-1} G_{ii}^T S F_{ii} + Q = 0$$
$$K_{dii} = (G_{ii}^T S G_{ii} + R)^{-1} G_{ii}^T S F_{ii}$$

An estimation of the state variables $x_i[k]$ is performed by a Kalman-Bucy observer [20], computed by:

$$\tilde{x}[k+1] = F\tilde{x}[k] + Gu[k] + L_d(y[k] - C\tilde{x}[k]) \quad (11)$$

where the $i-$th output of the microgrid is computed as $y_i[k] = C_{ii} x_i[k]$, being $y_i = v_i$ the PCC voltages, and where the observer gain matrix L_d is defined as

$$L_d = \begin{bmatrix} L_{d11} & L_{d12} & L_{d13} \\ L_{d21} & L_{d22} & L_{d23} \\ L_{d31} & L_{d32} & L_{d33} \end{bmatrix} \quad (12)$$

By considering a Linear-Quadratic-Regulator the L_d gain can be computed as

$$FSF^T - S - FSC^T(CSC^T + R)^{-1}CSF^T + Q = 0$$
$$L_d^T = (CSC^T + R)^{-1}CSF^T$$

It is worth mentioning that the constrains matrices Q and R are selected as identity matrices for computation of K_d, K_{dii} and L_d.

IV. HIL SYSTEM DESCRIPTION

The system is implemented by considering two Texas Instruments C2000 Microcontrollers Delfino TMS320F28379D in a configuration presented in Fig. 2.
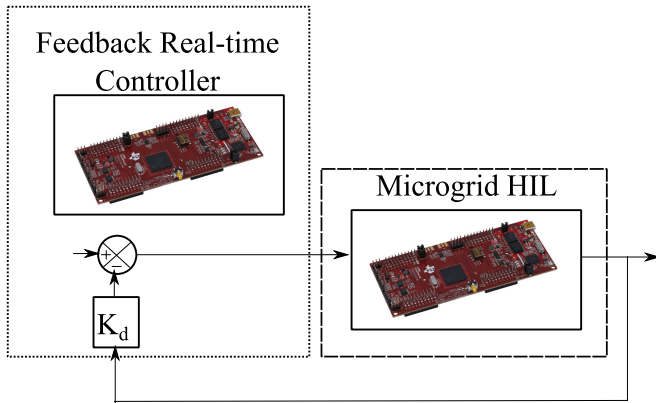
Fig. 2.   Real-time HIL structure for state feedback control

Fig. 4.   Real-time implementation of the centralized controller by using Simulink - Embedded Coder

The main features of the microcontrollers used can be described as:

1) 200 MHz dual C28x379 CPUs and dual CLAs,
2) 1 MB Flash
3) 16-bit/12-bit ADCs, comparators, 12-bit DACs

According to Fig. 2, a multivariable 3 inputs and 3 outputs microgrid system is simulated in one C2000 microcontroller by using 3 analog inputs and 3 analog outputs, and a a multivariable 3 inputs and 3 outputs state-feedback controller and Kalman-Buccy observer are simulated in the other C2000 microcontroller by using 3 analog inputs and 3 analog outputs.

In Fig. 3 is presented the microgrid system implemented in Simulink - Embedded Coder. The resulting code is implemented in the first C2000 Microcontroller.

Fig. 3.   Real-time implementation of the microgrid by using Simulink - Embedded Coder

In Fig. 4 is presented the centralized control system implemented in Simulink - Embedded Coder. The resulting code is implemented in the second C2000 Microcontroller. This centralized controller is used for a comparative analysis of the proposed approach.

In Fig. 5 is presented the proposed decentralized control approach implemented in Simulink - Embedded Coder. The resulting code is also implemented in the second C2000 Microcontroller.
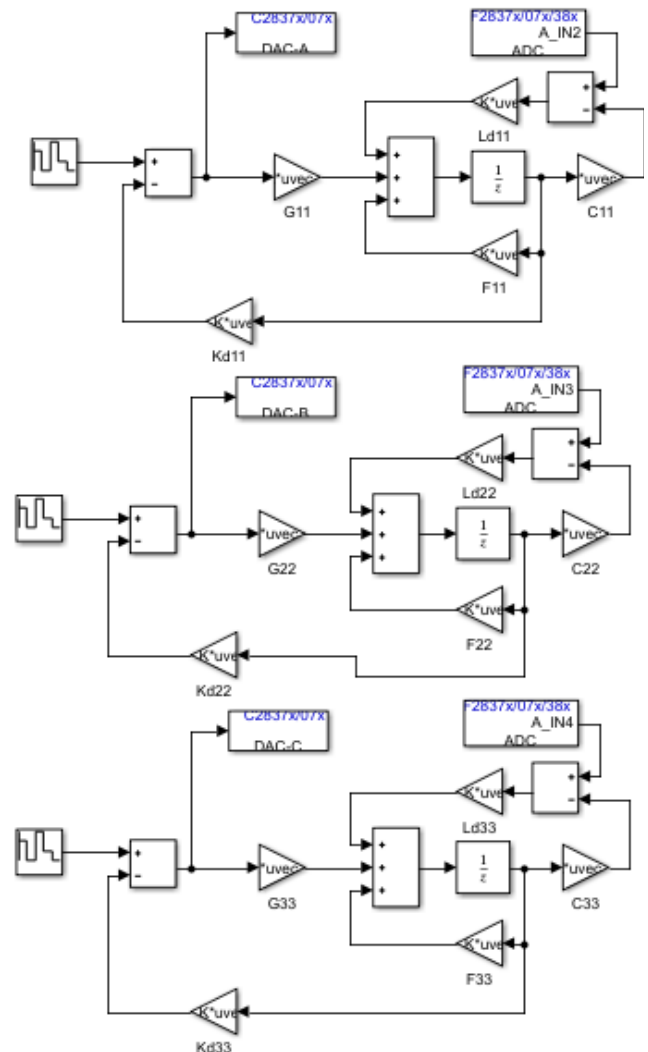

Fig. 5.   Real-time implementation of the decentralized controller by using Simulink - Embedded Coder

V. RESULTS

In order to evaluate the performance of the proposed decentralized control method, a comparison analysis is performed considering a centralized control. The comparison analysis is performed for states' behavior from initial conditions. The model of (7) is used for a HIL implementation of the system with a sample time $t_s = 0.5$ milliseconds. The performance is evaluated for a simulated environment by using Matlab and a real-time environment by using the HIL structure of Fig. 2. The values of microgrid elements are $R_{L1} = R_{L2} = R_{L3} = 1\Omega$, $R_{d1} = R_{d2} = R_{d3} = 1\Omega$, $R_{t1} = R_{t2} = 1\Omega$, $L_{L1} = L_{L2} = L_{L3} = 0.01H$, $L_{d1} = L_{d2} = L_{d3} = 0.01H$, $L_{t1} = L_{t2} = 0.01H$, $C_1 = C_2 = C_3 = 0.00001F$, $R_1 = R_2 = R_3 = 1\Omega$. And therefore, the discrete microgrid matrices are

$$F_{11} = F_{22} = \begin{bmatrix} 0.95 & 0 & 0 & 0.05 \\ 0 & 0.95 & 0 & -0.05 \\ 0 & 0 & 0.95 & 0.05 \\ -50 & -50 & -50 & -49 \end{bmatrix}$$

and

$$F_{33} = \begin{bmatrix} 0.95 & 0 & 0.05 \\ 0 & 0.95 & -0.05 \\ -50 & -50 & -49 \end{bmatrix}$$

with F_{11}, F_{22} and F_{33} the three microgrids feedback matrices, with inter-connections defined by the F_{ij} matrices, as follows

$$F_{12} = \begin{bmatrix} 0 & 0 & 0 & 0 \\ 0 & 0 & 0 & 0 \\ 0 & 0 & 0 & -0.05 \\ 0 & 0 & 0 & 0 \end{bmatrix}$$

and

$$F_{23} = \begin{bmatrix} 0 & 0 & 0 \\ 0 & 0 & 0 \\ 0 & 0 & -0.05 \\ 0 & 0 & 0 \end{bmatrix}$$

and $F_{13} = 0$, $F_{23} = 0$, $F_{31} = 0$ and $F_{32} = 0$. And also with

$$G_{11} = G_{22} = \begin{bmatrix} 0 \\ 0.05 \\ 0 \\ 0 \end{bmatrix}, G_{33} = \begin{bmatrix} 0 \\ 0.05 \\ 0 \end{bmatrix}$$

and $G_{12} = 0$, $G_{13} = 0$, $G_{21} = 0$, $G_{23} = 0$, $G_{31} = 0$ and $G_{32} = 0$.

The control signal for centralized control is computed according to (12) and where the estimated states are computed by (11), and where K_d is computed by using an optimal Linear Quadratic Regulator structure [12], with the following values for K_d

$$K_{d11} = \begin{bmatrix} -977.7 & -977.7 & -977.7 & -975.8 \end{bmatrix}$$
$$K_{d12} = \begin{bmatrix} -0.948 & -0.948 & -0.948 & -1.928 \end{bmatrix}$$
$$K_{d13} = \begin{bmatrix} 0.008 & 0.008 & 0.008 \end{bmatrix}$$
$$K_{d21} = \begin{bmatrix} 0.036 & 0.037 & 0.038 & 0.036 \end{bmatrix}$$
$$K_{d22} = \begin{bmatrix} -977.7 & -977.7 & -977.7 & -975.7 \end{bmatrix}$$
$$K_{d23} = \begin{bmatrix} -0.928 & -0.928 & -1.909 \end{bmatrix}$$
$$K_{d31} = \begin{bmatrix} 0.0039 & 0.0041 & 0.0045 & 0.004 \end{bmatrix}$$
$$K_{d32} = \begin{bmatrix} 0.0504 & 0.051 & 0.053 & 0.05 \end{bmatrix}$$
$$K_{d33} = \begin{bmatrix} -978.5 & -978.5 & -977.5 \end{bmatrix}$$

and the following values for L_d

$$L_{d11} = \begin{bmatrix} -48.35 \\ 48.35 \\ -48.37 \\ 48265.7 \end{bmatrix}, L_{d12} = \begin{bmatrix} -0.037 \\ 0.037 \\ 48.32 \\ 86.78 \end{bmatrix}, L_{d13} = \begin{bmatrix} 0.004 \\ -0.004 \\ 0.037 \\ -4.34 \end{bmatrix}$$

$$L_{d21} = \begin{bmatrix} 0.011 \\ -0.013 \\ 0.007 \\ -10.73 \end{bmatrix}, L_{d22} = \begin{bmatrix} -48.35 \\ 48.35 \\ -48.37 \\ 48265.0 \end{bmatrix}, L_{d23} = \begin{bmatrix} -0.034 \\ 0.033 \\ 48.37 \\ 83.15 \end{bmatrix}$$

$$L_{d31} = \begin{bmatrix} 0.003 \\ -0.004 \\ -3.76 \end{bmatrix}, L_{d32} = \begin{bmatrix} 0.015 \\ -0.018 \\ -14.71 \end{bmatrix}, L_{d33} = \begin{bmatrix} -48.39 \\ 48.39 \\ 48360.3 \end{bmatrix}$$

Results of simulation under noise conditions with random initial conditions are presented in Fig. 6 and Fig. 7 and Fig. 8 for centralized control.
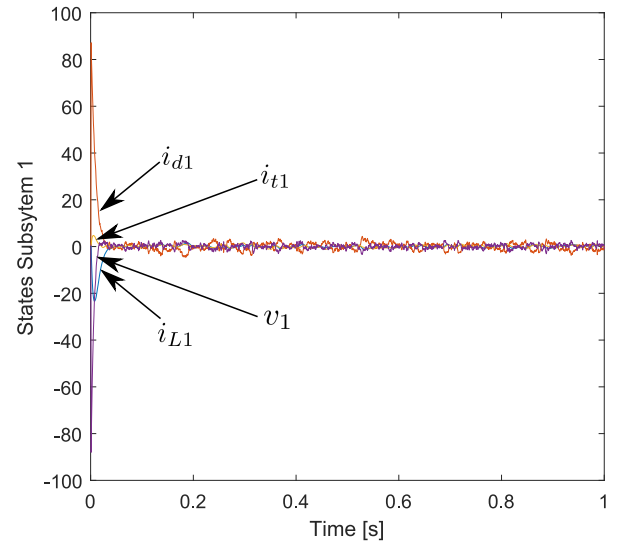

Fig. 6. Microgrid subsystem 1 simulated response to random initial conditions under noise environment
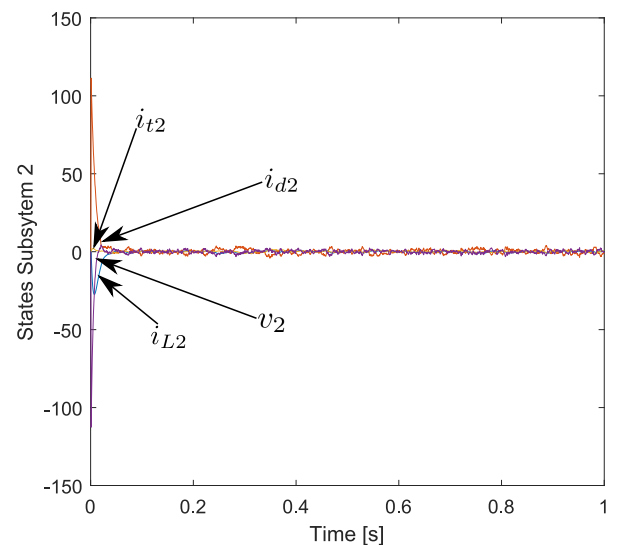

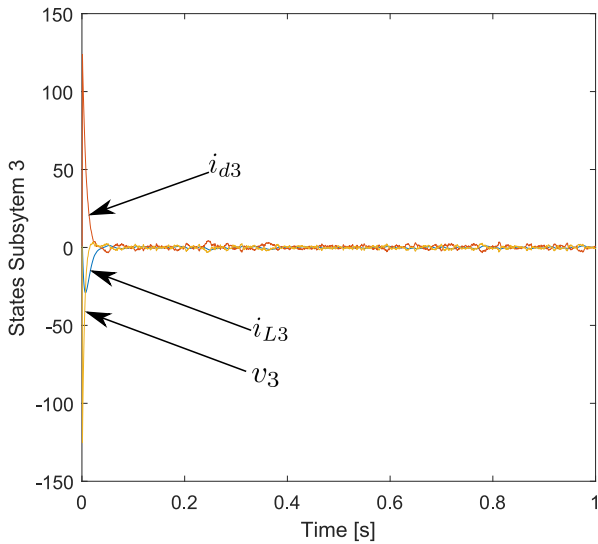Fig. 7. Microgrid subsystem 2 simulated response to random initial conditions under noise environment

Fig. 8.   Microgrid subsystem 3 simulated response to random initial conditions under noise environment
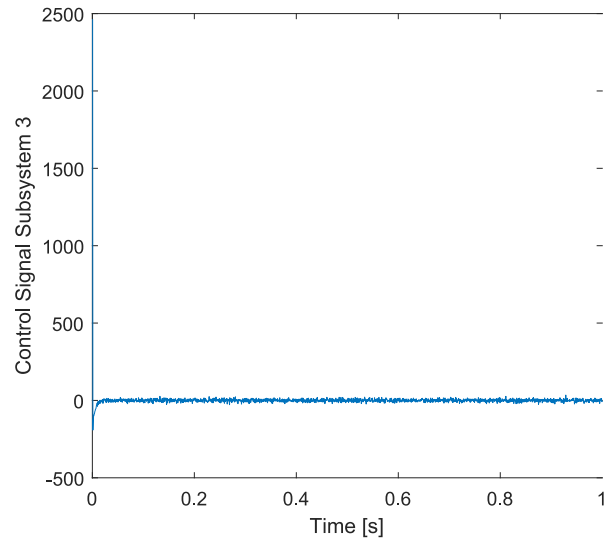
The corresponding control signals are shown in Fig. 9 and Fig. 10 and Fig. 11

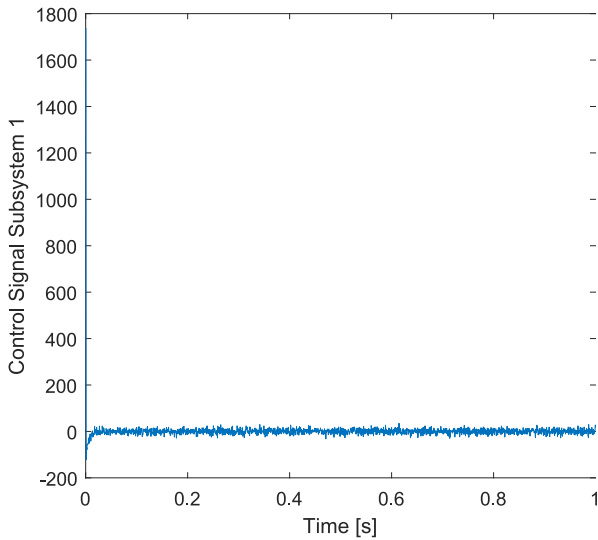Fig. 9.   Microgrid subsystem 1 simulated control signal

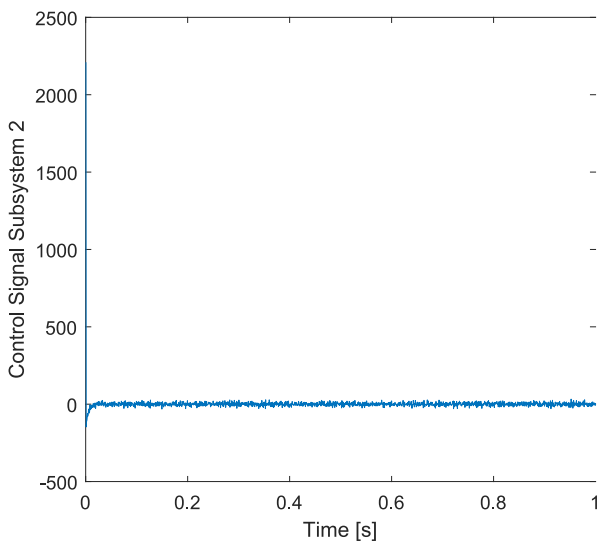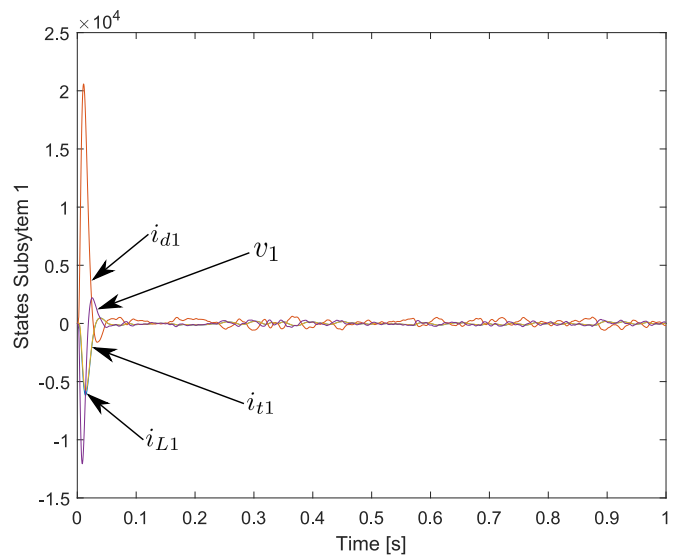Fig. 10.   Microgrid subsystem 2 simulated control signal

Fig. 11.   Microgrid subsystem 3 simulated control signal

Results of simulation under noise conditions with random initial conditions are presented in Fig. 12 and Fig. 13 and Fig. 14 for decentralized control. The control signal is computed considering

$$K_{d11} = \left[\begin{array}{cccc} -977.75 & -977.74 & -977.75 & -975.8 \end{array} \right]$$
$$K_{d22} = \left[\begin{array}{cccc} -977.75 & -977.74 & -977.75 & -975.8 \end{array} \right]$$
$$K_{d33} = \left[\begin{array}{ccc} -978.58 & -978.57 & -977.61 \end{array} \right]$$

being

$$K_d = \left[\begin{array}{ccc} K_{d11} & 0 & 0 \\ 0 & K_{d22} & 0 \\ 0 & 0 & K_{d33} \end{array} \right]$$

Fig. 12.   Microgrid subsystem 1 simulated decentralized response to random initial conditions under noise environment
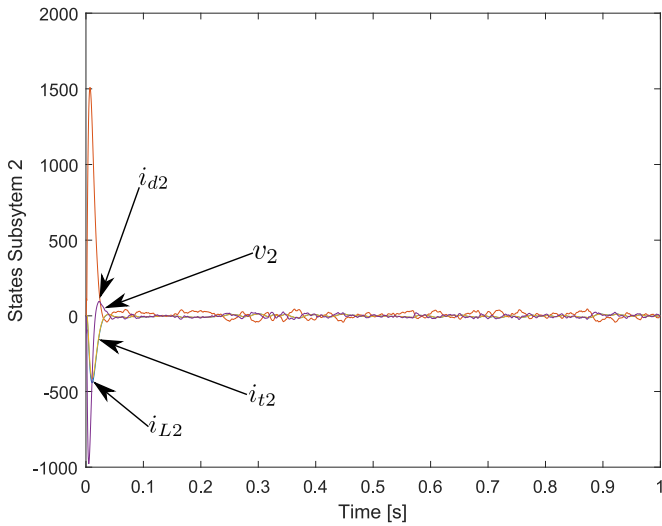
Fig. 13. Microgrid subsystem 2 simulated decentralized response to random initial conditions under noise environment
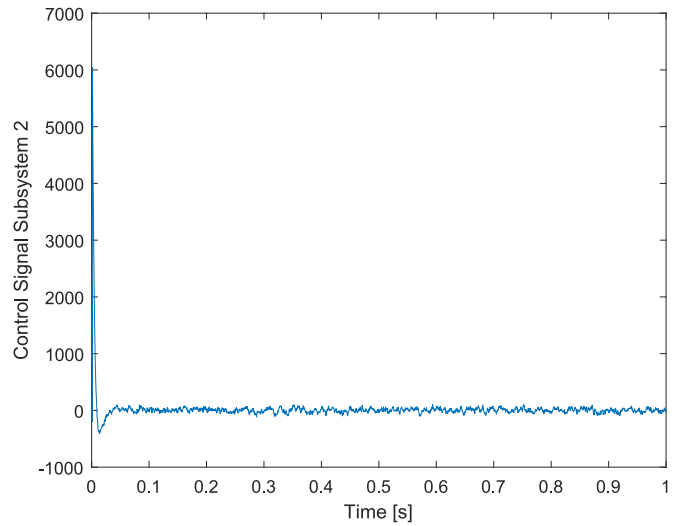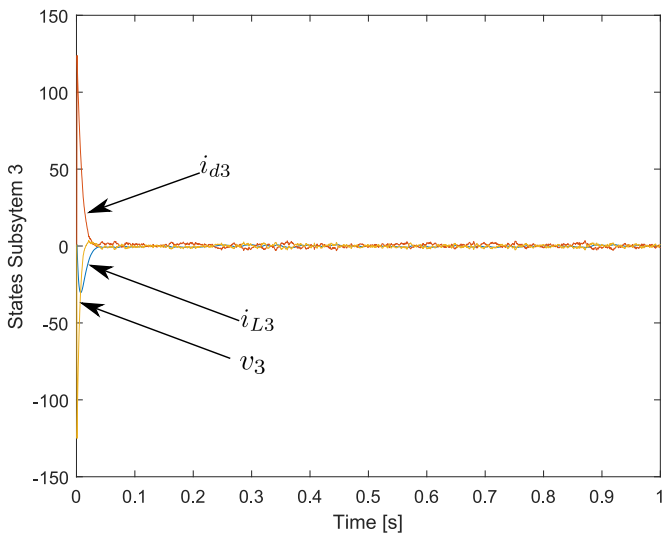

Fig. 14. Microgrid subsystem 3 simulated decentralized response to random initial conditions under noise environment

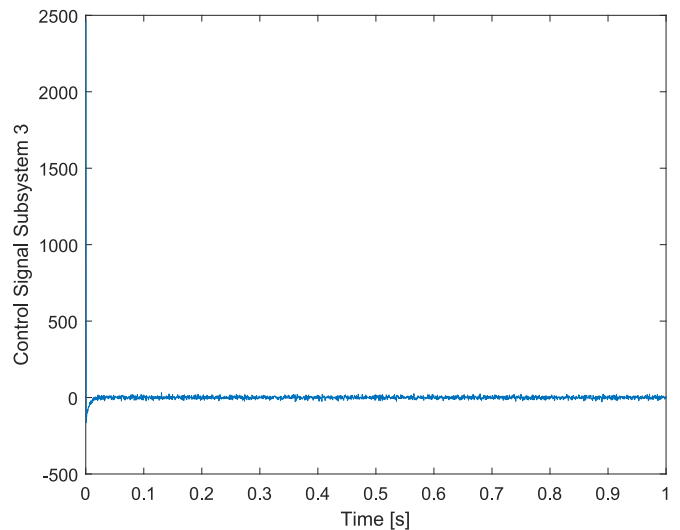The corresponding control signals are shown in Fig. 15 and Fig. 16 and Fig. 17

Fig. 15. Microgrid subsystem 1 simulated control signal decentralized

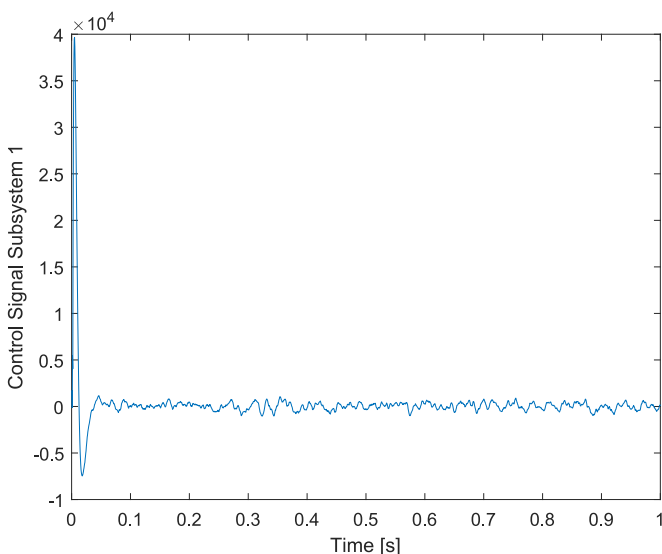Fig. 16. Microgrid subsystem 2 simulated control signal decentralized

Fig. 17. Microgrid subsystem 3 simulated control signal decentralized

For reference tracking, the following control signal is defined

$$u[k] = -K_d x[k] + K_g r[k] \qquad (13)$$

being $K_g = (C(I - F + GK)^{-1}G)^{-1}$ as follows

$$K_g = \begin{bmatrix} -0.0799 & 0.0304 & -0.00026 \\ -0.00021 & -0.08159 & 0.0298 \\ 0.00014 & -0.00056 & -0.0553 \end{bmatrix}$$

The corresponding output signals for a reference tracking changing from 0V to 12 V at time 0.5 seconds are shown in Fig. 18 and Fig. 19 and Fig. 20
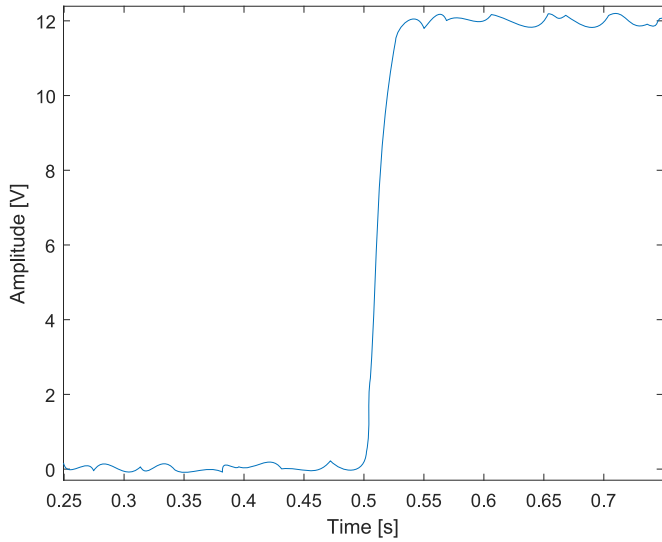
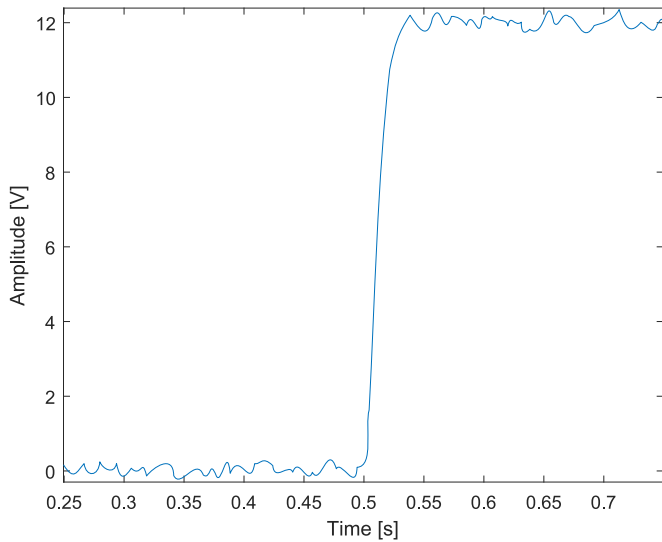Fig. 18.   Microgrid subsystem 1 output signal for reference tracking

Fig. 19.   Microgrid subsystem 2 output signal for reference tracking
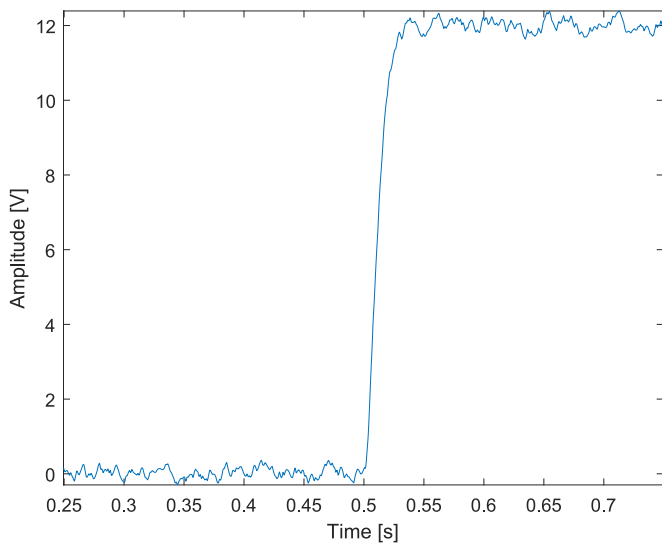

Fig. 20.   Microgrid subsystem 3 output signal for reference tracking

In addition, the proposed approach is evaluated over a HIL structure, where the centralized and decentralized results are depicted in Fig. 21, Fig. 22, Fig. 23 for centralized and Fig. 24, Fig. 25, Fig. 26 for decentralized. The data is acquired by using the USB port where the selected sample time is 0.5 milliseconds.
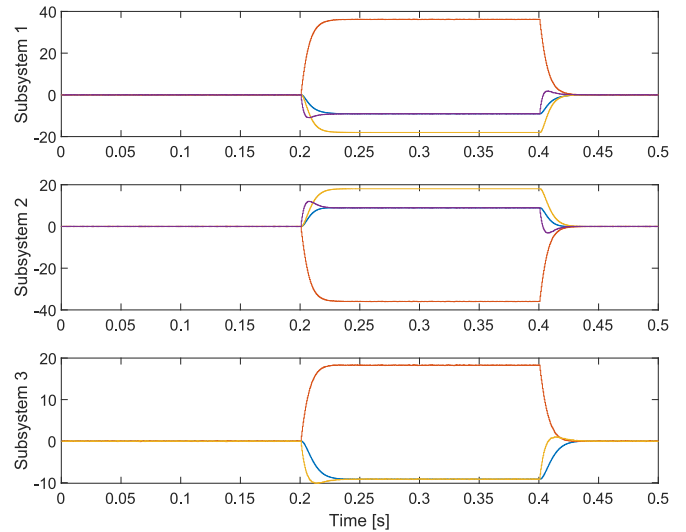

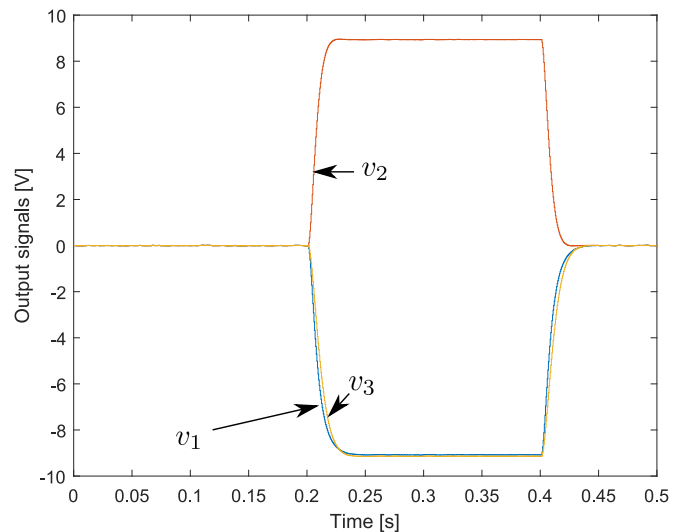Fig. 21.   Microgrid states real-time HIL centralized control

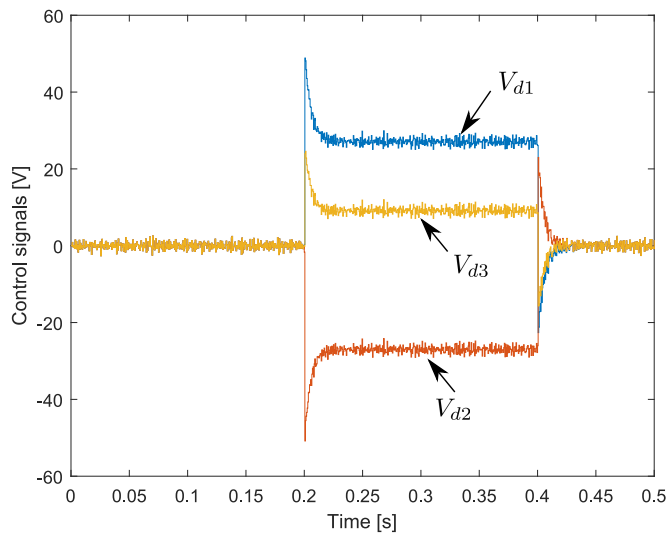Fig. 22.   Microgrid outputs real-time HIL centralized control

Fig. 23.   Microgrid control signals real-time HIL centralized control

Fig. 24.   Microgrid states real-time HIL decentralized control

Fig. 25.   Microgrid outputs real-time HIL decentralized control
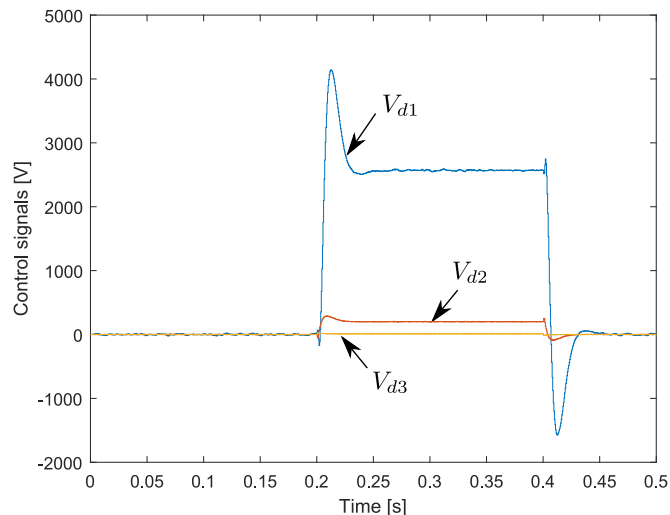
Fig. 26.   Microgrid control signals real-time HIL decentralized control

A visualization of $y_1[k]$ and $u_1[k]$ obtained for the decentralized proposed approach is also presented in Fig. 27 by scaling the input and output data in the 0V to 3.3V range and by using a UNI-T Oscilloscope of 100MHz bandwidth with a 1GS/s sample rate.
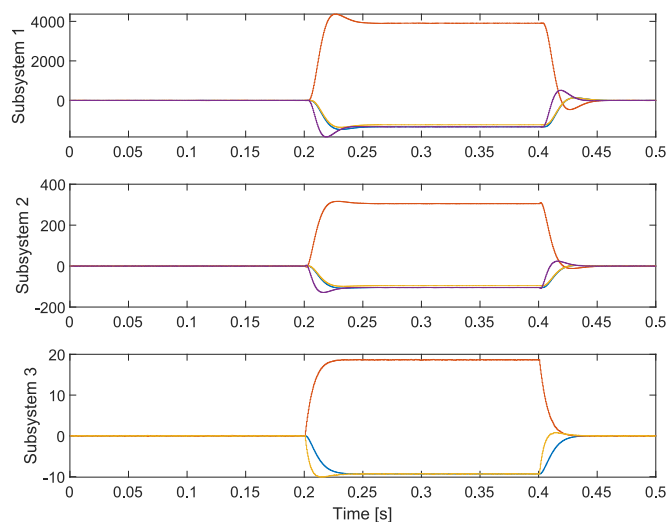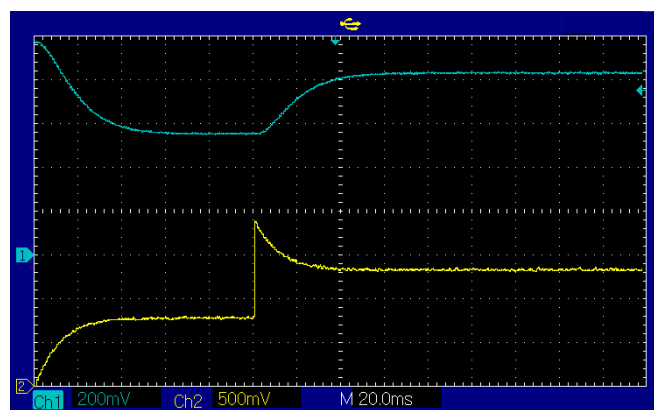
Fig. 27.   Oscilloscope visualization of $y_1[k]$ (blue line) and $u_1[k]$ (yellow line) mapped in the 0V to 3.3V range

From Fig. 27 it can be seen that the settling-time achieved from an initial point is around $t_S = 40$ milliseconds.

VI. CONCLUSIONS

A novel method for real-time evaluation of microgrids control structures is proposed. Two methods are compared: the proposed approach for decentralized control of the microgrid, based on a state estimation Kalman-Bucy structure, and a centralized approach controller. It can be seen that the states are estimated by using only one measurement for each subsystem of the microgrid where closed-loop stability is obtained. In addition, it is worth mentioning that the feedback gains for centralized and decentralized approaches are computed by using a Linear Quadratic Regulator approach. It is worth noting that the validation performed using the HIL structure allows the extension of the results obtained to a real application.

REFERENCES

[1] J. C. Vasquez, J. M. Guerrero, J. Miret, M. Castilla, and L. G. de Vicuña, "Hierarchical control of intelligent microgrids," *IEEE Industrial Electronics Magazine*, vol. 4, no. 4, pp. 23–29, 2010.
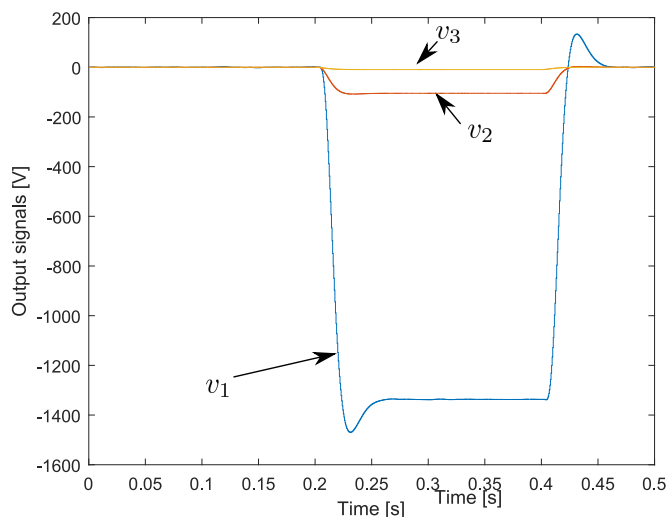
[2] D. C. Silva Júnior, J. G. Oliveira, P. M. de Almeida, and C. Boström, "Control of a multi-functional inverter in an ac microgrid – real-time simulation with control hardware in the loop," *Electric Power Systems Research*, vol. 172, pp. 201–212, 2019. [Online]. Available: https://www.sciencedirect.com/science/article/pii/S0378779619301099

[3] S. Tan, Y. Wu, P. Xie, J. M. Guerrero, J. C. Vasquez, and A. Abusorrah, "New challenges in the design of microgrid systems: Communication networks, cyberattacks, and resilience," *IEEE Electrification Magazine*, vol. 8, no. 4, pp. 98–106, 2020.

[4] H. Mo and G. Sansavini, "Real-time coordination of distributed energy resources for frequency control in microgrids with unreliable communication," *International Journal of Electrical Power and Energy Systems*, vol. 96, pp. 86–105, 2018. [Online]. Available: https://www.sciencedirect.com/science/article/pii/S0142061517311912

[5] Q. L. Lam, A. I. Bratcu, D. Riu, C. Boudinet, A. Labonne, and M. Thomas, "Primary frequency h control in stand-alone microgrids with storage units: A robustness analysis confirmed by real-time experiments," *International Journal of Electrical Power and Energy Systems*, vol. 115, p. 105507, 2020. [Online]. Available: https://www.sciencedirect.com/science/article/pii/S0142061518334604

[6] A. Mammoli, M. Robinson, V. Ayon, M. Martinez-Ramon, C. fei Chen, and J. M. Abreu, "A behavior-centered framework for real-time control and load-shedding using aggregated residential energy resources in distribution microgrids," *Energy and Buildings*, vol. 198, pp. 275–290, 2019. [Online]. Available: https://www.sciencedirect.com/science/article/pii/S0378778818329074

[7] G. C. Goodwin and K. S. Sin, *Adaptive Filtering, Prediction and Control*. Englewood-Cliffs: Dover Publications Inc., 2009.

[8] F. Osorio-Arteaga, D. Giraldo-Buitrago, and E. Giraldo, "Sliding mode control applied to mimo systems," *Engineering Letters*, vol. 27, no. 4, pp. 802–806, 2019.

[9] E. Giraldo, *Multivariable Control*. Germany: Scholar's Press, 2016.

[10] C. D. Molina-Machado and E. Giraldo, "Bio-inspired control based on a cerebellum model applied to a multivariable nonlinear system," *Engineering Letters*, vol. 28, no. 2, pp. 464–469, 2020.

[11] F. Osorio-Arteaga, J. J. Marulanda-Durango, and E. Giraldo, "Robust multivariable adaptive control of time-varying systems," *IAENG International Journal of Computer Science*, vol. 47, no. 4, pp. 605–612, 2020.

[12] J. S. Velez-Ramirez, M. Bueno-Lopez, and E. Giraldo, "Adaptive control approach of microgrids," *IAENG International Journal of Applied Mathematics*, vol. 50, no. 4, pp. 802–810, 2020.

[13] C. Hu, Y. Wang, S. Luo, and F. Zhang, "State-space model of an inverter-based micro-grid," in *2018 3rd International Conference on Intelligent Green Building and Smart Grid (IGBSG)*, 2018, pp. 1–7.

[14] M. Rana, L. Li, and S. Su, "Kalman filter based microgrid state estimation and control using the iot with 5g networks," in *2015 IEEE PES Asia-Pacific Power and Energy Engineering Conference (APPEEC)*, 2015, pp. 1–5.

[15] M. Rana, L. Li, and S. W. Su, "Microgrid state estimation and control using kalman filter and semidefinite programming technique," *International Energy Journal*, vol. 16, pp. 47–56, 2016.

[16] S. A. Taher, M. Zolfaghari, C. Cho, M. Abedi, and M. Shahidehpour, "A new approach for soft synchronization of microgrid using robust control theory," *IEEE Transactions on Power Delivery*, vol. 32, no. 3, pp. 1370–1381, 2017.

[17] T. Suehiro and T. Namerikawa, "Decentralized control of smart grid by using overlapping information," in *2012 Proceedings of SICE Annual Conference (SICE)*, 2012, pp. 125–130.

[18] J. S. Velez-Ramirez, L. A. Rios-Norena, and E. Giraldo, "Buck converter current and voltage control by exact feedback linearization with integral action," *Engineering Letters*, vol. 29, no. 1, pp. 168–176, 2021.

[19] M. M. Rana and L. Li, "An overview of distributed microgrid state estimation and control for smart grids," *Sensors*, vol. 15, no. 2, pp. 4302–4325, 2015. [Online]. Available: https://www.mdpi.com/1424-8220/15/2/4302

[20] M. S. Rahimi Mousavi and B. Boulet, "Dynamical modeling and optimal state estimation using kalman-bucy filter for a seamless two-speed transmission for electric vehicles," in *2015 23rd Mediterranean Conference on Control and Automation (MED)*, 2015, pp. 76–81.